Effect of chlorine on water incorporation in magmatic amphibole: experimental constraints with a micro-Raman spectroscopy approach

Enrico Cannaò, Federica Schiavi, Giulia Casiraghi, Massimo Tiepolo, Patrizia Fumagalli

Eur. J. Mineral., 34, 19–34, 2022
https://doi.org/10.5194/ejm-34-19-2022

European Journal of Mineralogy
Open Access

Effect of chlorine on water incorporation in magmatic amphibole: experimental constraints with a micro-Raman spectroscopy approach

Enrico Cannaò[1], Federica Schiavi[2], Giulia Casiraghi[1], Massimo Tiepolo[1], and Patrizia Fumagalli[1]

[1]Dipartimento di Scienze della Terra "A. Desio", Università di Milano, Via S. Botticelli 23, 20133 Milan, Italy
[2]Université Clermont-Auvergne, CNRS, IRD, OPGC, Laboratoire Magmas et Volcans, 63000 Clermont-Ferrand, France

Correspondence: Enrico Cannaò (enrico.cannao@unimi.it)

Received: 22 July 2021 – Revised: 19 November 2021 – Accepted: 1 December 2021 – Published: 21 January 2022

Abstract. Amphibole represents an important repository of water (among other volatiles, e.g., chlorine and fluorine) in the lithosphere in all those environments characterized by the circulation of fluids and hydrous melts, such as subduction zones and subcontinental lithospheric mantle. Therefore, detailed knowledge of the mechanisms ruling water incorporation in amphibole is essential to assess the amount of water that can be fixed in the lithosphere by this mineral and, ultimately, gain a better insight into the deep water cycle. Water is incorporated into the structure of amphibole as hydroxyl (OH^-), which is hosted in the anion site $O(3)$, and the incorporation is mainly controlled by the oxo-substitution mechanism ${}^{M(1)}Ti_1^{4+} + {}^{O(3)}O_2^{2-}\ {}^{M(1)}(Mg^{2+}, Fe^{2+})_{-1} + {}^{O(3)}(OH^-)_{-2}^-$. However, the fluids and melts circulating in the lithospheric mantle can be variably enriched in halogens (Cl^- and F^-) that can substitute OH^- in the anion site $O(3)$ of amphibole, thus potentially affecting its water budget.

The aim of this study is to evaluate the effect of Cl on the oxo-substitution and the incorporation of water in amphibole. End-loaded piston cylinder experiments were conducted at pressure and temperature conditions compatible with the upper-mantle depth (1.4 GPa and 1015–1050 °C) in order to favor the crystallization of amphibole at equilibrium with the coexisting melt. Alkali basalt powder was used as starting material, and water doped with different contents of Cl was added to each experiment. Two ranges of oxygen fugacity (fO_2) were investigated at $\Delta FMQ = -2.6$ ($\log fO_2$ [experiment] $-$ $\log fO_2$ [FMQ buffer]) and $\Delta FMQ = +1.7$, where FMQ is fayalite–magnetite–quartz, in order to preliminarily identify the potential influence of the fO_2 on the water budget in amphibole. In this contribution, we propose a new method to quantify water in amphiboles using confocal micro-Raman spectroscopy.

The H_2O contents range from 2.20 ± 0.10 wt % to 5.03 ± 0.47 wt % in glasses and from 0.93 ± 0.08 wt % to 1.50 ± 0.12 wt % in amphiboles, resulting in a partition coefficient of water between amphibole and glass (${}^{Amph/L}D_{H_2O}$) ranging from 0.29 ± 0.06 to 0.52 ± 0.08. Our results show a positive correlation between the Cl content of amphibole (from 0.18 wt % to 0.88 wt %) and the ${}^{Amph/L}D_{H_2O}$. This effect is ascribed to the incorporation of Cl at the anion site $O(3)$ that influences the oxo-substitution mechanism by impeding the entrance of Ti^{4+} at the $M(1)$ sites and thus preventing the amphibole dehydrogenation.

The effect of Cl reported in this study, which is related to a change in the amphibole crystal structure, highlights that high Cl concentrations in magmatic systems favor the incorporation of water in amphibole rather than in the coexisting melt, although the exchange coefficient between ${}^{Amph/L}D_{H_2O}$ and ${}^{Amph/L}D_{Cl}$ supports a preferential incorporation of water over Cl in amphibole. Therefore, the presence of abundant Cl influences the hydration state of magmas evolving from upper-mantle conditions towards crustal roots with the crystallization of amphibole.

Published by Copernicus Publications on behalf of the European mineralogical societies DMG, SEM, SIMP & SFMC.

1 Introduction

Amphibole, although a minor mineral in the Earth's mantle system, represents an important repository of volatile elements and in particular of water. Amphibole occurs in a variety of geological environments characterized by circulation of fluids and hydrous melts, and its stability might exert a primary role in the storage and/or release of volatiles at depth (Dawson and Smith, 1982; O'Reilly and Griffin, 1988; Mandler and Grove, 2016). Amphibole can be found in subduction-related mantle rocks, where it is a recurring phase in both the mantle wedge and the lower to middle crust of the overriding plate (Coltorti et al., 2007; Davidson et al., 2007; Ionov and Hofmann, 1995; Marocchi et al., 2007; Smith, 2014), and it is also widespread in the subcontinental lithospheric mantle either as disseminated mineral or in veins (Demény et al., 2005; Peters et al., 2017; Vannucci et al., 1995). Upper-mantle amphiboles have been found in ultramafic (peridotitic or pyroxenitic) xenoliths or as xenocrysts embedded in alkaline lavas, scoria, and maars (e.g., Campbell and Schenk, 1950; Varne, 1970; Francis, 1976; Takahashi, 1980; Dawson and Smith, 1982; Griffin et al., 1984; Press et al., 1986; Fabriès et al., 1987; Dautria et al., 1987; Field et al., 1989; Mayer et al., 2014) as well as in orogenic massifs, i.e., upper-mantle fragments tectonically emplaced within crustal terrains during continent–continent collision (e.g., Green, 1964; Cawthorn, 1975; Ernst, 1978; Medaris, 1980, 1984; Obata, 1980; Obata and Morten, 1987; Seyler and Mattson, 1989; Rampone and Morten, 2001). These amphiboles are generally kaersutites and Ti-rich pargasite, according to the nomenclature of Leake et al. (1997).

A common feature of high-temperature (T) amphiboles, such as kaersutite and Ti-rich pargasite, is their H deficiency to different degrees (Dawson and Smith, 1982; Hawthorne et al., 2012; Vannucci et al., 1995). The loss of H from the crystal lattice during crystallization occurs by deprotonation (i.e., release of H^+) of the hydroxyl anion OH^- hosted at the $O(3)$ site. Deprotonation takes place mainly via the following local mechanism (Demény et al., 2006; King et al., 1999; Popp et al., 1995b, 2006):

$$^{M(1)}\mathrm{Ti}_1^{4+} + {}^{O(3)}\mathrm{O}_2^{2-} {}^{M(1)}(\mathrm{Mg}^{2+}, \mathrm{Fe}^{2+})_{-1} + {}^{O(3)}(\mathrm{OH})^-_{-2}. \quad (1)$$

With this exchange mechanism, referred to as Ti oxo-substitution, the cation hosted in the octahedral $M(1)$, usually Mg^{2+} or Fe^{2+}, is substituted by Ti^{4+}, and the charge balance within the structure is maintained by deprotonation of two OH^- hydroxyls at the $O(3)$ sites. Various parameters including pressure (P), T, composition of the system, oxygen fugacity (fO_2), and hydrogen fugacity (fH_2) influence reaction (1) and, thus, determine the OH^- content in amphibole during crystallization (Dyar et al., 1992; Popp et al., 1995a; King et al., 1999; Oberti et al., 2007).

The water content in natural igneous amphiboles can however be modified after crystallization due to additional partial dehydrogenation during slow cooling of amphibole in near-surface (i.e., volcanic) environments, where finally fH_2 differs from the initial one (Clowe et al., 1988; King et al., 1999). This mechanism is given by the following oxidation reaction:

$$^{M(1,3)}\mathrm{Fe}_1^{3+} + {}^{O(3)}\mathrm{O}_1^{2-} + 1/2\mathrm{H}_2 {}^{M(1,3)}\mathrm{Fe}^{2+}_{-1} + {}^{O(3)}\mathrm{OH}^-_{-1}. \quad (2)$$

Dehydrogenation at $O(3)$ is a consequence of oxidation of Fe^{2+} to Fe^{3+} at the $M(1)$ and $M(3)$ sites. The release of H^+ takes place to balance the excess positive charge generated by the oxidation process. Remarkably this dehydrogenation mechanism can be active also in upper-mantle regions when the redox conditions of the system allow the incorporation of a high amount of Fe^{3+} in the crystal structure of amphibole.

Chlorine (Cl) in amphibole can substitute for OH^- at the $O(3)$ site: the difference in ionic radius between Cl and OH^- (1.81 vs. 1.37 Å, respectively; Shannon, 1976) implies significant modification in the entire amphibole crystal structure (Makino et al., 1993; Oberti et al., 1993, 2007; Hawthorne and Oberti, 2007) with consequences for the Ti oxo-substitution (1) and, ultimately, for the incorporation of water in amphibole. The occurrence of Cl-rich amphiboles at mantle depths has been documented in several geological settings (e.g., Frezzotti et al., 2010; Piper et al., 2019), although no information concerning their water content is reported.

An important parameter to evaluate the affinity of water for amphibole (i.e., water incorporation) is the partition coefficient of water between amphibole and the coexisting liquid ($^{\mathrm{Amph/L}}D_{H_2O} = [H_2O]_{\mathrm{Amph}}/[H_2O]_{\mathrm{L}}$). This parameter may constrain variations in the capability of amphibole to incorporate water as a consequence of the modification of the system composition. All the parameters that may affect or control the water incorporation in hydrous minerals must be defined and clearly separated from post-crystallization processes. In this frame, we experimentally synthesized amphiboles at 1.4 GPa (i.e., upper level of mantle conditions) in a chemically controlled system, avoiding post-crystallization modifications. We investigated the effect of Cl content of the system on the $^{\mathrm{Amph/L}}D_{H_2O}$. High-$T$ experiments at Earth's upper-mantle conditions produced amphiboles coexisting with andesitic melts. Micro-Raman spectroscopy was adopted to quantify the water content of run products, applying a novel statistical approach (e.g., Bolfan-Casanova et al., 2014) to amphiboles for the first time. In addition, two ranges of fO_2 were investigated at $\Delta\mathrm{FMQ} = -2.6$ ($\log fO_2$ [experiment] $- \log fO_2$ [FMQ buffer]) and $\Delta\mathrm{FMQ} = +1.7$, where FMQ is fayalite–magnetite–quartz, in order to preliminarily identify the potential influence of the oxygen fugacity on the incorporation of water in amphibole. This contribution is part of a wider project aimed at investigating trace element

partitioning between amphibole and liquid at Earth's upper-mantle conditions (Cannaò et al., 2022).

2 Experimental procedures

A synthetic glass (47-N; Tiepolo et al., 2000) analog to an alkali basalt was used as starting material. It was prepared using reagent-grade oxides, carbonates, and metals, resembling the alkaline–olivine basalt 4722-13a of Wedepohl (1983). The starting material was doped in several trace elements (e.g., REE, LILE, and HFSE) of geological significance (Tiepolo et al., 2000). In order to attain the saturation of the system and, thus, promote amphibole crystallization, 1000 ppm of ICP standard solutions was used as a source for some trace elements (As and Sb) and added to ultrapure (i.e., type I) water (Cannaò et al., 2022). Chlorine was added to the system with the Sb solution at the 2 % level.

Experiments were carried out at the Laboratory of Experimental Petrology of the Dipartimento di Scienze della Terra "A. Desio" (University of Milan, Italy) using an end-loaded piston cylinder apparatus. Run conditions are shown in Table 1. The experimental charges run at 1.4 GPa and T ranging from 1050 to 1015 °C using an MgO–Pyrex–talc assembly. Pressure is considered to be accurate to 3 % and temperature ±5 °C. Runs were heated up to 1300 °C and maintained at this T, i.e., at supra-liquidus conditions, for 1 h. Then the system was cooled down at a rate of 0.5 °C/min to the experimental equilibrium T and kept for 12 h. In order to approach amphibole liquidus and favor large, possibly unzoned amphiboles, different equilibrium T values around a narrow interval (1050 to 1015 °C; Tiepolo et al., 2000) were chosen. This experimental procedure was adopted in order to promote the growth of amphibole crystals instead of their nucleation and to reach equilibrium between amphibole and coexisting melt. Quench was obtained by turning off the power supply, which resulted in an initial quench rate of approximately 90 °C/s.

The first set of experiments, labeled with C (47-N 17-7C, 17-4C, and 17-9C), were conducted with a single Pt outer capsule enclosing an inner graphite capsule containing the sample (i.e., starting material powder plus water). This assembly permits fO_2 to be maintained close to the C-CO–CO_2 equilibrium during the whole run (CCO; Ulmer and Luth, 1991), which is about $\Delta\text{FMQ} = -2.6$ at our experimental conditions. Graphite is also used to isolate the sample from the Pt capsule and avoid Fe loss (Johannes and Bode, 1978). For experiments 17-7C and 17-9C we used a Pt capsule with an inner diameter (ID) of ∼ 2.8 mm, whereas for experiment 17-4C the Pt capsule has an ID of ∼ 4.5 mm.

In the second set of experiments, denominated HM, higher fO_2 was fixed at about $\Delta\text{FMQ} = +1.7$, combining the hematite–magnetite (HM) solid buffer with the double-capsule technique (17-8HM; Ganguly and Newton, 1968) or the triple-capsule technique (18-15HM; Matjuschkin et al., 2015). The double capsule consists of a single Fe pre-saturated Pt capsule (ID ∼ 2.0 mm), loaded with the starting material, and an outer-welded Pt capsule filled with fine hematite powder plus ∼ 30 % of ultrapure water (i.e., buffering assemblage). In the triple-capsule technique both sample and buffering assemblages were seal-welded into two separated Fe pre-saturated Pt capsules (ID ∼ 2.0 mm) and then placed inside a third outer-welded Pt capsule (ID ∼ 2.0 mm) filled with Al_2O_3 plus ultrapure water. It should be noted that the intrinsic fugacity of the end-loaded piston cylinder apparatus coupled with the use of talc in the assembly leads to the partial reduction in the hematite into magnetite (Ulmer and Luth, 1991) in both experimental configurations. As long as hematite and magnetite coexist, this buffer fixes the fO_2 of the experimental runs at $\Delta\text{FMQ} = +1.7$ (for further details see also Cannaò et al., 2022).

3 Analytical techniques

3.1 Electron microprobe

Experimental run products were investigated for major element composition by the JEOL Superprobe 8200 electron microprobe (EMP) at the Dipartimento di Scienze della Terra, Università di Milano (Italy). The following natural standards were used: olivine for Mg, fayalite for Fe, omphacite for Na, ilmenite for Ti, K-feldspar for K, anorthite for Al and Ca, wollastonite for Si, pure Cr for Cr, scapolite for Cl, and niccolite for Ni. Beam conditions were 15 kV accelerating voltage and 5 nA current. The beam size was 1 µm for clinopyroxene and amphibole phases and up to 3 µm for the glass and mica. Counting time was 10 s for background and 30 s for the peak.

3.2 Micro-Raman spectroscopy

Water in amphiboles and glasses was determined by polarized micro-Raman spectroscopy. The analyses were carried out at the Laboratoire Magmas et Volcans (Clermont-Ferrand) using an inVia confocal micro-Raman spectrometer with a backscattered configuration designed by Renishaw and equipped with a 532.1 ± 0.3 nm diode laser (output power: 200 mW), a Peltier-cooled charge-coupled device (CCD) detector, a Rayleigh rejection edge filter, and a Leica DM 2500M optical microscope with a motorized XYZ stage. We used a high confocal setting (20 µm slit aperture), a 100× microscope objective and a grating of 2400 grooves/mm. This setting resulted in lateral and axial spatial resolutions of ∼ 1 and 2–3 µm at the sample surface and allowed a spectral resolution of $\sim 0.5\,\text{cm}^{-1}$. Laser power on the sample was reduced by filters to operate at 8 mW power. The spectra were acquired with polarized light using a half-wave plate. For water quantification in amphiboles and glasses, standards and samples were analyzed using the same analytical conditions. Daily calibration of the spectrometer was performed on a silicon standard ($520.5\,\text{cm}^{-1}$ peak).

Table 1. Run conditions and phase assemblages for all the experiments.

Run no.	T (°C)	Nominal H_2O (wt %)	fO_2	Anhydrous glass composition	Phase assemblage*	Sum of square of residual
17-7C	1015	5.0	CCO	Trachyandesite	cpx[25] + amph[40] + (mica, ilm)[<1] + liq[34]	0.24
17-4C	1015	13.0	CCO	Andesite	cpx[38] + amph[32] + (mica, ilm)[<1] + liq[28]	1.41
17-9C	1040	13.2	CCO	Trachyandesite	cpx[34] + amph[32] + (ilm)[<1] + liq[36]	1.53
17-8HM	1050	6.5	HM	Trachyandesite	cpx [35] + amph[25] + (ilm)[<1] + liq[39]	1.18
18-15HM	1050	8.8	HM	Trachyandesite	cpx [28] + amph[24] + (ilm)[<1] + liq[47]	1.00

* Numbers in square brackets are the modes of each phase calculated with a least squares linear regression mass balance. CCO: C–CO–CO_2 buffer; HM: hematite–magnetite buffer. Minerals in round brackets are only present as accessory phases. Mineral abbreviations: cpx – clinopyroxene, amph – amphibole, ilm – ilmenite, liq – glass.

The spectra were recorded using WiRE™ 4.2 software in the wavenumber ranges from ~ 50 to $1300\,cm^{-1}$ and from ~ 2900 to $3900\,cm^{-1}$, which represent the vibration regions of the alumino-silicate network and of the O–H bond stretching, respectively. A total of 4 and 8 to 12 acquisitions of 15 s each were collected in the alumino-silicate and water spectral regions, respectively. After acquisition, cubic and linear baselines were fit to the spectra, respectively, in the water and alumino-silicate regions using PeakFit package software. Then the integrated intensities (i.e., the area) under the water peak (A_{OH}) and the silicate region (A_{Si}) were obtained and normalized to 1 s and 1 mW. The ratio A_{OH}/A_{Si} was calculated for each acquired spectrum.

For quantification of water in glasses, an external calibration method was used following the procedure described in Schiavi et al. (2018). A total of 5 to 10 measurements were carried out on each sample. Basaltic, andesitic, and rhyolitic glasses with different water contents were used as reference standards (Médard and Grove, 2008; Schiavi et al., 2018) and analyzed several times during each analytical session in order to correct for the dependence of band intensities on delivered energy.

Due to the anisotropy of the amphibole and its complex structure, shape and intensity of Raman bands vary significantly from one crystal to another as a function of the orientation of the crystal lattice relative to the polarization plane of the laser source (Fig. 1). Consequently, the spectrum acquired on one polished face of a crystal is not fully representative of its water content. The method used to quantify water in amphibole adopts a statistical approach similar to that described by Bolfan-Casanova et al. (2014) for measuring water content in olivine using micro-Raman spectroscopy. In this approach, measurements are taken on a large number of amphibole grains differently oriented in two dimensions so that the average of these measurements simulates the analysis performed on individual standard amphiboles that are rotated and analyzed in three orthogonal directions. In each sample, several amphibole crystals, generally comprised of between 10 and 20 (but only 6 in the sample 18-15HM), were measured along different crystallographic orientations. Two measurements along orthogonal directions were taken systematically in each analyzed crystal to limit the effect of a potential preferential crystallographic orientation within the sample (Martinek and Bolfan-Casanova, 2021). Then average A_{OH} and A_{OH}/A_{Si} values for amphiboles were calculated in each sample and converted to water contents using the calibration lines defined by the amphibole standards with known water contents (Fig. 2).

Four kaersutitic amphibole crystals from Arizona (USA; Campbell and Schenk, 1950) and one kaersutitic amphibole collected from pyroclastites in the Ardèche volcanic province (France) were used as standards for the calibrations (Fig. 2). The five crystals were examined and oriented under a binocular microscope: they display prismatic habitus elongated parallel to the c axis, with the (110) face generally well developed and evident cleavage planes intersecting at 124 and 56° (Deer et al., 1997). The method used to build the calibration is based on the theoretical considerations developed for quantitative absorbance measurements in anisotropic crystals by Libowitzky and Rossman (1996). These authors demonstrated that quantitative spectroscopic measurements in anisotropic media can be accomplished from polarized spectra on either three random, but orthogonal sections of a crystal or two orthogonal sections oriented parallel to each of the two axes of the indicatrix ellipsoid. As for the monoclinic amphiboles, orienting the crystals parallel to the axes of the optical indicatrix is no trivial task because only one of these three axes coincides with one of the crystallographic axes (Deer et al., 1997), i.e., the b axis. Therefore, in each kaersutite standard we made measurements on three orthogonal sections: the basal section perpendicular to the c axis and two planes parallel to the c axis, either the (100) and (010) faces or the (110) face and a plane orthogonal to it. If originally absent or not well developed, these planes were created by sectioning and polishing the crystal along defined directions. A large number of micro-Raman spectra were acquired (54 in total on 3 orthogonal faces; Fig. 1) by aligning the edge of each face with the instrument polarization axis and then rotating the crystal from 0 to 180° in steps of 10° each. Then the average values of A_{OH} and A_{OH}/A_{Si} for the three faces taken together were calculated and used to build the calibration lines (Fig. 2). The uncertainty (standard deviation, 1σ) associated with the micro-Raman data is the result of errors related to (i) the analytical measurements; (ii) the

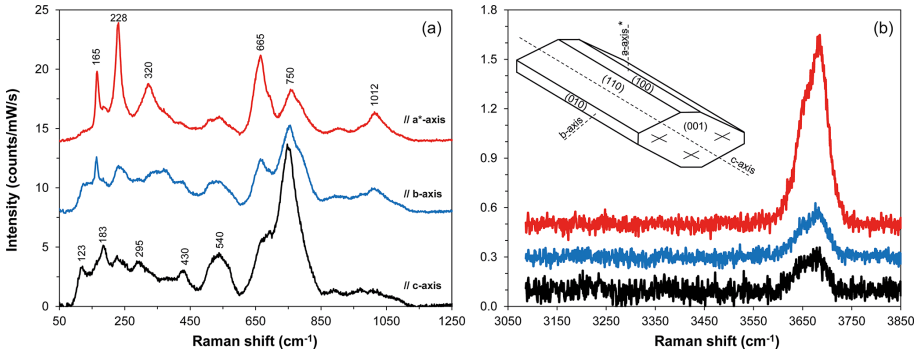

Figure 1. Polarized Raman spectra of the amphibole standard MGT4 in the regions of silicate network **(a)** and O–H stretching **(b)** vibrations, after baseline correction, as a function of the orientation of the crystal lattice relative to the polarization direction of the laser beam. The polarization of incident light was parallel to the polarization of scattered light. Polarized spectra were acquired on three orthogonal sections (100, 010, and 001). Representative spectra shown from bottom to top were collected, respectively, with the direction of laser polarization parallel to the *c* axis, *b* axis, and *a* axis*. The *a* axis* is distinguished from the true *a* axis because it is perpendicular to *b* axis and *c* axis. Note that the directions of the *a* axis and *c* axis do not coincide with those of the optical indicatrix axes in monoclinic amphiboles. The (top) spectrum with the most intense peaks at 228 and 665 cm^{-1} displays the strongest OH band, whereas the (bottom) spectrum with the maximum peak at 750 cm^{-1} is associated with the smallest OH band. Raman intensity was normalized to laser power and acquisition time. Spectra are vertically offset for clarity.

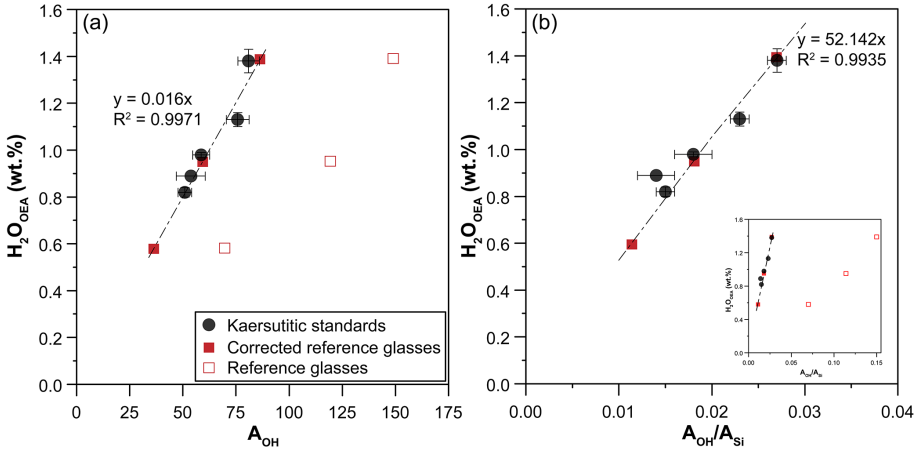

Figure 2. Calibration lines defined by kaersutitic amphiboles used as standards: correlation between water contents of amphibole determined by the OEA and **(a)** A_{OH} or **(b)** A_{OH}/A_{Si}. The three reference glasses also used as external standards during all Raman sessions are plotted. The factors used to correct the intensities of the reference glasses are reported in Table 3.

dispersion of the relative intensities of the vibrational modes caused by the anisotropy of the minerals, which is intrinsic to the statistical method used for water quantification (Martinek and Bolfan-Casanova, 2021); and (iii) micro-Raman spectra treatment procedures (e.g., baseline fitting). The relative uncertainty is about 10 % and 12 % for amphiboles and glasses, respectively.

The spectral analysis of the kaersutitic standards revealed that the spectra displaying the most intense peak near 750 cm^{-1} (see black spectrum in Fig. 1a) represent ∼ 67 % of all spectra acquired in each standard, the other ∼ 33 % being associated with the spectra showing the most intense peak at 228 cm^{-1} and, to a lesser extent, at 665 cm^{-1}. Therefore, we took 67 % as a reference value to assess the level of randomness of the orientations used for water quantification on the samples, as detailed later in the text.

3.3 Organic elemental analyzer (OEA)

Water content of the five amphibole standards was determined by CHNS analyses (Organic Elemental Analyzer Flash 2000, Thermo Fisher) at the University of Milan and at the Laboratoire Magma et Volcans (Clermont-Ferrand). Samples were dried overnight to avoid any contamination with air humidity. Three measurements were performed for each standard.

4 Experimental run products: phase assemblages, textures, and mineral chemistry

Run results together with run conditions are shown in Table 1. Glass is the ubiquitous phase in run products, indicating that all experiments were run at supra-solidus conditions. Amphibole crystallized as a stable phase in all experiments where it is associated with clinopyroxene and traces of oxides (ilmenite). On occasion, in experiments 17-4C and 17-7C, traces of mica were found but always in textural disequilibrium with both amphibole and clinopyroxene and the glass (Fig. 3). All the runs display similar textural features: (i) clinopyroxene and amphibole are embedded in an abundant glass matrix; (ii) clinopyroxene (100 to 300 µm in dimension) shows anhedral habitus and evident zoning; and (iii) amphibole, as both single crystals and overgrowing former clinopyroxene crystals, displays euhedral habitus with a crystal size ranging from less than 50 up to 350 µm in sections parallel to the c axis. Little chemical zoning within amphibole crystals is shown near small glass inclusions. The presence of spherical holes in the glass matrix in each experiment likely suggests the achievement of water saturation conditions of the system. Based on the textural relations observed among phases, the following crystallization sequence is inferred: clinopyroxene ± (mica) ± amphibole ± oxide. Phase abundances were derived by mass balance calculations using a weighted least squares minimization procedure (Table 1). Major oxides included in the mass balance calculations are SiO_2, Al_2O_3, TiO_2, MgO, FeO, CaO, Na_2O, and K_2O. For the purpose of the mass balance calculation, all iron has been assumed as Fe^{2+} as the global ferric/ferrous ratio in the run charges is unknown, although a moderate Fe^{3+} amount can be contained in both clinopyroxene and amphibole.

The major element compositions of the experimental products are reported in Table 2. Glass composition mainly falls in the trachyandesite and andesite fields in the TAS diagram (Fig. 4a). A general increase in the Mg# (i.e., Mg value) and TiO_2 at increasing T is observed. Glasses in experiments conducted at the same T and fO_2 conditions but different nominal H_2O contents show different major element compositions. In fact, the glass of experiment 17-7C (1015 °C, CCO buffer, 5.0 wt % H_2O) has higher Mg# and CaO, K_2O, and TiO_2 contents and lower SiO_2 and Al_2O_3 contents compared to the glass of experiment 17-4C (1015 °C, CCO buffer, 13.0 wt % H_2O). Likewise, the glass of experiment 17-8HM (1050 °C, HM buffer, 6.5 wt % H_2O) has higher SiO_2 and Al_2O_3 and lower CaO and TiO_2 contents compared to the glass of experiment 18-15HM (1050 °C, HM buffer, 8.8 wt % H_2O). By comparing the experiments 17-4C and 17-9C, carried out at the same fO_2 conditions (CCO buffer) and H_2O contents (about 13.0 wt %) but different T (1015 and 1040 °C, respectively), an increase in Mg#, CaO, alkali, and TiO_2 can be observed with increasing temperature, accompanied by a decrease in SiO_2 and Al_2O_3. A key feature of these glasses is their variable and high concentration in Cl ranging from 0.74 ± 0.04 wt % to 2.40 ± 0.07 wt %.

According to the classification of Leake et al. (1997), crystallized amphiboles span in composition from kaersutite to Fe-kaersutite with subordinate pargasite and Fe-pargasite in the experiment 17-7C (Fig. 4b). The positive correlation described by the Mg# of amphibole and glasses from each experiment (Fig. 5) falls on the same trend provided in Tiepolo et al. (2000), suggesting chemical equilibrium between these phases (see also Cannaò et al., 2022). Similarly to glasses, synthesized amphiboles show high Cl content ranging from 0.18 ± 0.01 wt % to 0.88 ± 0.09 wt %. The relationship between Cl content in amphibole coexisting with glass shows a positive linear trend (Fig. 6a). A positive linear correlation is also observed between TiO_2 and Cl contents in amphibole (Fig. 6b), which appears to be dependent on the fO_2 condition of the system.

The clinopyroxene composition is in between augite and diopside in all experiments, whereas the micas identified in experiments 17-4C and 17-7C span in composition between annite and biotite, respectively. As these phases are unstable with the surrounding glasses (Fig. 3), no further chemical presentation is provided.

5 Determination of water contents by micro-Raman spectroscopy

5.1 Calibration of water contents in amphibole standards

Micro-Raman spectra of kaersutitic amphibole standards display bands at ∼ 123, 165, 183, 228, 295, 320, 370, 430, 540, 665, 750, and 1012 cm^{-1} (Fig. 1a). Relative intensities of the Raman bands of kaersutite strongly depend on the crystallographic orientation (Figs. 1, S1 in the Supplement), with the most intense peaks occurring at ∼ 228, 665, and 750 cm^{-1}. The strong Raman scattering near 750 cm^{-1} is indicative of oxo-amphiboles and is related to the high number of Ti–O bonds (Leissner et al., 2015). The spectra in the OH region show a broad band located between 3600 and 3750 cm^{-1}, which consists of two or more components, with the most intense component centered near 3685 cm^{-1} (Fig. 1b); the area of the OH bond (A_{OH}) varies significantly according to the orientation (Figs. 1b, S1).

The values of A_{OH} and A_{OH}/A_{Si} (Fig. 2) show a linear correlation with the water contents (expressed as H_2O) of the kaersutite standards ranging from 0.82 wt % to 1.38 wt %, as determined by the OEA (Table 3). Therefore, these calibration lines can be used to determine the water content of unknown amphibole crystals. Following the method proposed by Bolfan-Casanova et al. (2014), we repeatedly analyzed three reference glasses with different water contents (Médard and Grove, 2008; Schiavi et al., 2018) throughout the Raman sessions in order to use them as external calibrants

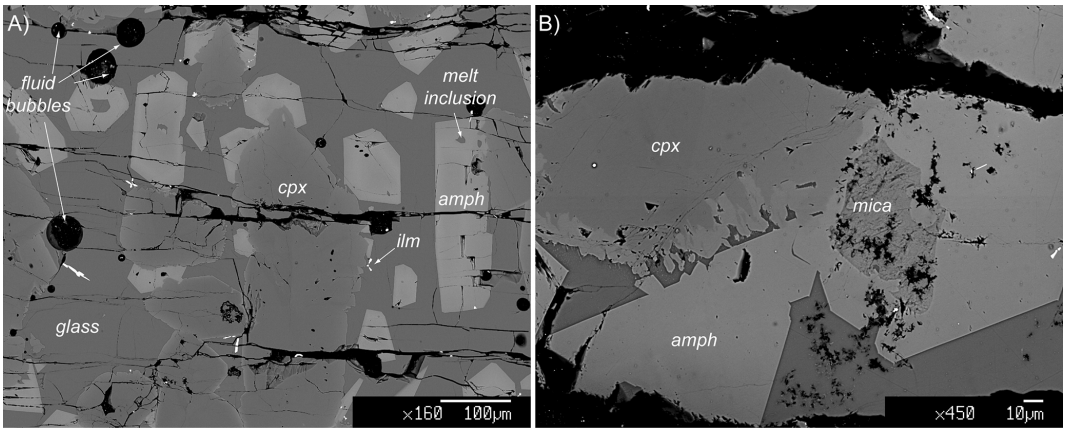

Figure 3. Representative backscattered electron (BSE) images showing the key textural relationship in experimental runs. Clinopyroxene (cpx) is always infiltrated by the melt matrix and partially overgrown amphibole (amph). Amphibole shows a polygonal habit, suggesting chemical equilibrium with the surrounding glass matrix. Sometimes small pockets of melt inclusion and former crystals of mica are present within amphibole crystals. Ilm: ilmenite. **(a)** Experiment 17-4C, **(b)** experiment 17-7C.

instead of kaersutitic standards, thus allowing us to reduce the time required for daily analysis of standards. The three glasses plot far from the linear calibrations defined by the kaersutites (Fig. 2), meaning that the Raman cross-section of these glasses is very different from that of the amphiboles and that correction factors for glass intensities are needed to align glasses and amphiboles on the same line. In other words, both A_{OH} and A_{OH}/A_{Si} of glass standards must be multiplied by the correction factors reported in Table 3 in order to fall on the regression lines defined by the kaersutite standards. The correction factors include differences in composition, density, refractive index, and absorptivity (Bolfan-Casanova et al., 2014; Thomas et al., 2008) compared to amphiboles. After correction, these glass standards can be used as external calibrants for quantification of water in kaersutitic amphiboles.

5.2 Water contents in synthesized glasses and amphiboles

The H_2O contents range from 2.20 ± 0.10 wt % to 5.03 ± 0.47 wt % in glasses and from 0.93 ± 0.08 wt % to 1.50 ± 0.12 wt % in amphiboles (Table 4, Fig. 7a). Representative micro-Raman spectra of glasses and amphiboles are shown in the Supplement (Figs. S2 and S3). In three samples, the percentage of amphibole spectra displaying the most intense peak near 750 cm^{-1} does not differ much from that of the amphibole standards: 58 % of all acquired spectra in sample 17-7C, 69 % in sample 17-9C, and 73 % in 17-8HM. The spectra showing the strongest peak at 228 cm^{-1} sum up to about 30 %, with the others associated with the highest peak at 665 cm^{-1}. This observation indicates that the sampling of various crystal orientations (i.e., the extent of anisotropy sampled) was good in these samples. In the sample 17-4C the percentage of spectra with maximum intensity at 750 cm^{-1} increases to 86 %, likely because of a subtle preferential orientation of the amphiboles within the capsule. Instead, in the sample 18-15HM, where a small number (6) of amphibole crystals was available for analyses, the spectra with the most intense peak near 750 cm^{-1} sum up to 50 % of the total spectra, while the other 50 % are represented by spectra having the most intense peak at 665 or 228 cm^{-1}. We used the reference value of 67 % provided by the analyses on the kaersutitic standards to correct the water contents estimated for the amphiboles of samples 17-4C and 18-15HM. For this correction, a weighted average for A_{OH} (and A_{OH}/A_{Si}) was calculated, imposing a contribution of 67 % to the spectra with maximum intensity at 750 cm^{-1} and of 33 % to differently oriented spectra. The corrected values are provided in Table 4.

A significant negative correlation trend is shown between the content of H_2O and TiO_2 in amphiboles (Fig. 7b), potentially related to the Ti oxo-substitution mechanisms, and negative trends are shown in a H_2O_{amph} vs. Cl_{amph} diagram (Fig. 7c), likely due to their competition at the $O(3)$ site of the amphibole (see "Discussion").

6 Discussion

6.1 Approach to equilibrium

In order to evaluate the approach to equilibrium, both textural relationships and chemical phase homogeneity of run products have been evaluated. As shown in Fig. 3, amphibole crystallizes directly from the melt forming single crystals embedded in the glass or develops on clinopyroxene as a rim. In both cases, the euhedral habitus of amphiboles suggests the equilibrium with the coexisting melt. Major element homogeneity within amphibole crystals was assessed by mea-

Table 2. Average major element (wt %) composition of run products.

Exp no.	17-4C							
Phase	Amphibole	SD	Clinopyroxene	SD	Mica	SD	Glass	SD
n (no. of analyses)	29		25		5		15	
SiO_2	37.95	0.60	49.77	2.01	35.29	0.29	57.94	0.61
TiO_2	5.87	0.64	1.46	0.64	9.96	0.22	0.96	0.10
Al_2O_3	16.38	0.47	8.13	2.28	16.36	0.27	18.14	0.19
FeO_{Tot}	17.49	1.42	7.28	1.43	15.93	1.22	6.17	0.41
MgO	6.94	1.16	14.74	1.88	9.85	0.67	0.85	0.08
CaO	9.35	0.23	17.39	1.26	0.10	0.04	2.66	0.12
Na_2O	2.69	0.12	1.07	0.23	0.76	0.04	3.31	0.08
K_2O	1.69	0.12	0.01	0.01	8.50	0.04	2.70	0.06
Cl	0.58	0.14	<0.01		0.32	0.03	1.32	0.06
Total	98.94		99.84		97.05		90.44	
Exp no.	17-7C							
Phase	Amphibole	SD	Clinopyroxene	SD	Mica	SD	Glass	SD
n (no. of analyses)	16		15		4		15	
SiO_2	39.08	0.37	51.54	1.20	36.20	0.32	52.35	0.57
TiO_2	4.38	0.33	1.05	0.35	6.51	0.21	1.34	0.14
Al_2O_3	15.12	0.24	5.83	1.45	16.68	0.58	16.46	0.29
FeO_{Tot}	14.94	0.37	6.10	1.17	11.93	0.51	7.14	0.25
MgO	8.97	0.42	15.35	1.74	13.81	0.34	1.49	0.16
CaO	10.18	0.11	19.10	0.77	0.08	0.02	4.67	0.12
Na_2O	2.66	0.05	0.86	0.19	0.80	0.05	3.46	0.14
K_2O	1.61	0.04	0.01	0.01	8.73	0.04	3.46	0.08
Cl	0.31	0.02	<0.01		0.20	0.01	1.26	0.03
Total	97.26		99.85		94.92		91.62	

Exp no.	17-9C					
Phase	Amphibole	SD	Clinopyroxene	SD	Glass	SD
n (no. of analyses)	24		25		20	
SiO_2	37.25	0.28	49.82	1.54	53.77	0.22
TiO_2	6.83	0.50	1.37	0.50	1.59	0.11
Al_2O_3	16.68	0.33	7.59	1.76	17.91	0.16
FeO_{Tot}	14.89	0.39	6.20	1.03	7.74	0.19
MgO	8.39	0.38	15.71	1.48	1.51	0.07
CaO	9.18	0.34	17.50	0.96	4.28	0.06
Na_2O	2.67	0.13	1.00	0.17	3.69	0.09
K_2O	1.76	0.12	0.01	0.01	4.00	0.06
Cl	0.88	0.09	<0.01		2.40	0.07
Total	98.54		99.20		96.89	

suring electron microprobe (EMP) line profiles across some grains, whereas homogeneity of amphibole and glass within each experiment was checked by observing the variability in EMP analysis acquired at random spots throughout the capsule (see Cannaò et al., 2022). Additionally, Mg–Fe partitioning between glasses and amphiboles is consistent with bulk X_{Mg} of the starting glass and follows a T-dependent positive correlation (Fig. 5), in agreement with previous experiments of Tiepolo et al. (2000). Mass balance analysis further supports constraints against macroscopic fractionation within the charge, as expected in static fluid-saturated experiments (Schmidt and Ulmer, 2004). Further evidence of the achievement of equilibrium is based on trace element concentrations as reported in Cannaò et al. (2022; see their Fig. 5).

Table 2. Continued.

Exp no.	17-8HM					
Phase	Amphibole	SD	Clinopyroxene	SD	Glass	SD
n (no. of analyses)	22		27		40	
SiO_2	38.74	1.31	50.42	1.03	57.09	0.67
TiO_2	6.09	0.77	1.28	0.37	1.60	0.14
Al_2O_3	16.28	0.67	7.24	0.96	19.74	0.25
FeO_{Tot}	10.02	0.81	3.96	0.47	3.62	0.31
MgO	11.67	0.52	15.82	0.71	1.50	0.18
CaO	9.96	1.57	19.22	0.39	3.50	0.22
Na_2O	2.90	0.26	1.11	0.12	3.77	0.14
K_2O	1.59	0.37	0.01	0.01	3.89	0.06
Cl	0.29	0.08	<0.01		0.99	0.06
Total	97.53		99.06		95.69	
Exp no.	18-15HM					
Phase	Amphibole	SD	Clinopyroxene	SD	Glass	SD
n (no. of analyses)	3		20		16	
SiO_2	39.52	0.63	51.04	0.79	52.40	0.88
TiO_2	4.70	0.37	1.06	0.22	2.20	0.17
Al_2O_3	15.56	0.08	6.10	0.78	17.53	0.23
FeO_{Tot}	10.05	0.55	5.07	0.60	5.32	0.47
MgO	12.29	0.36	15.87	0.69	2.71	0.23
CaO	10.32	0.20	19.01	0.55	5.34	0.18
Na_2O	2.58	0.14	0.92	0.09	3.22	0.10
K_2O	1.62	0.10	0.01	0.01	3.41	0.10
Cl	0.18	0.01	<0.01		0.74	0.04
Total	96.81		99.07		92.86	

Table 3. Water content of the amphibole standards and reference glasses.

		H (wt %)	1σ	H_2O	
Kaersutite	MGT1	0.125	0.003	1.126	
Kaersutite	MGT2	0.109	0.001	0.977	
Kaersutite	MGT3	0.092	0.002	0.824	
Kaersutite	MGT4	0.099	0.001	0.889	
Kaersutite	BV007	0.154	0.005	1.376	
		H_2O (wt %)	1σ	A_{OH} corr.factor	A_{OH}/A_{Si} corr.factor
Basaltic glass	82-72f#19	0.580	0.050	0.527	0.16
Basaltic glass	82-72f#10	1.390	0.080	0.564	0.18
Andesitic glass	A030417	0.950	0.050	0.514	0.16

MGT: Hoover Dam (Arizona, USA). BV: Bas-Vivarais volcanic province (Ardèche, France). Reference glass compositions are reported in Schiavi et al. (2018)

6.2 Ti oxo-substitution, Fe^{3+}/Fe_{tot} ratio, and OH incorporation in amphibole

The negative correlation between TiO_2 and H_2O content (Fig. 7b) strongly suggests that Ti oxo-substitution (1) is the dominant mechanism controlling the water content in the studied amphiboles. However, the significantly lower water content of amphibole in experiment 17-8HM (1050 °C) compared to experiments with similar TiO_2 content, such as 17-4C and 17-9C (1015 and 1040 °C, respectively) (Figs. 6b, 7b), suggests that the dehydrogenation mechanism (2) is also active, as already pointed out by Adam et al. (2007).

More oxidizing conditions, as in experiment 17-8HM, produce amphibole with higher Fe^{3+}/Fe_{tot} (up to 0.106, Table 5)

Table 4. Mean H_2O contents in amphibole and glass determined by Raman spectroscopy in each experiment and calculated partition coefficients for H_2O and Cl ($^{Amph/L}D_{H_2O}$ and $^{Amph/L}D_{Cl}$, respectively).

Experimental run	H_2O_{amph}	1σ	H_2O_{glass}	1σ	$^{Amph/L}D_{H_2O}$	1σ	$^{Amph/L}D_{Cl}$	1σ
17-4C	1.25	0.12	2.41	0.23	0.52	0.08	0.439	0.107
17-7C	1.50	0.12	5.03	0.47	0.30	0.04	0.248	0.017
17-9C	1.14	0.08	2.20	0.10	0.52	0.04	0.368	0.040
17-8HM	0.93	0.08	2.36	0.11	0.39	0.04	0.291	0.079
18-15HM	1.23	0.10	4.21	0.52	0.29	0.06	0.244	0.016

Cl content (wt %) in amphiboles and glasses is reported in Table 2.

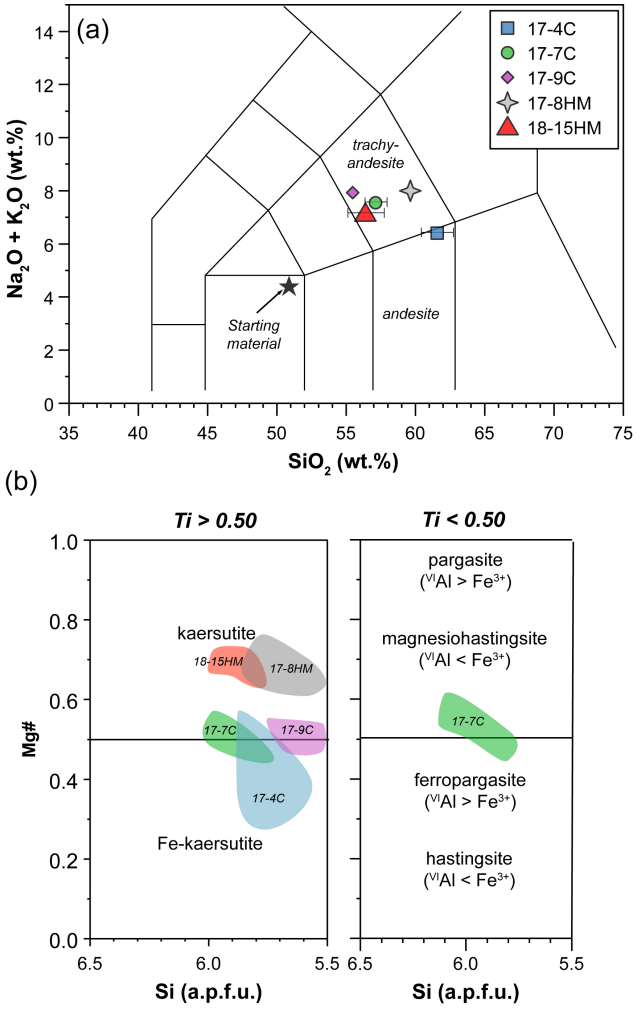

Figure 4. **(a)** Major element composition of glass (TAS diagram – normalized to anhydrous 100 wt %) and **(b)** Mg value (Mg# = Mg + Fe/Mg) versus Si (a.p.f.u.) of amphibole (according to classification of Leake et al., 1997). Labels in **(b)** refer to the experimental runs (see Table 1).

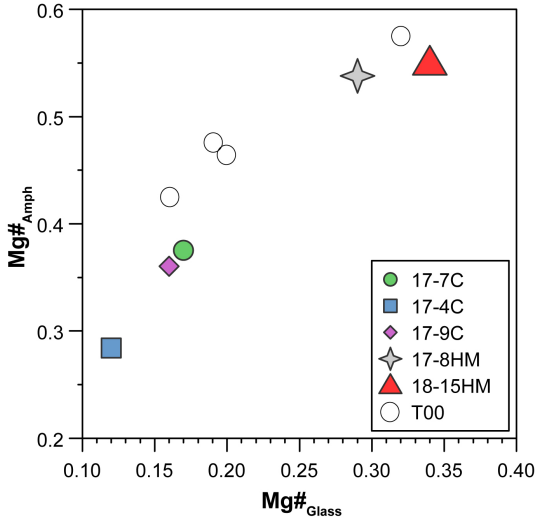

Figure 5. Positive correlation between Mg# of amphiboles and glasses suggesting conditions close to equilibrium. T00: data from Tiepolo et al. (2000).

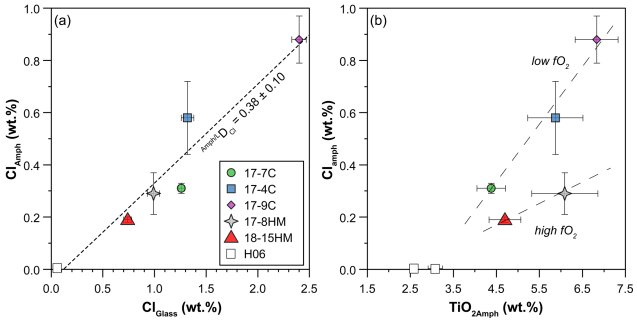

Figure 6. **(a)** Positive correlation between Cl content (wt %) in amphiboles and glasses reflecting the high Cl content of the system. The dashed line is the trend line of all data (this study and the literature), and its slope indicates the $^{Amph/L}D_{Cl}$. **(b)** Positive correlation between Cl and TiO_2 content (wt %) in amphiboles pointing to their interdependence, which appears to be related to fO_2 of the system. Dashed lines in **(b)** are a visual guide. H06: data from Hauri et al. (2006).

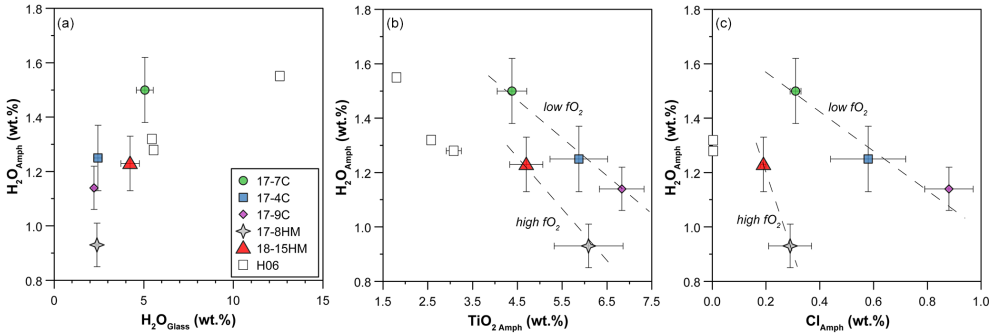

Figure 7. (a) Relation between H_2O contents (wt %) in amphiboles and quenched melt. Correlation between H_2O content (wt %) in amphibole and its TiO_2 **(b)** and Cl **(c)** contents (wt %). In **(c)** two separated correlations are visible based on the fO_2 of the system (dashed lines are a visual guide). H06: data from Hauri et al. (2006).

as compared to amphibole synthesized at fO_2 close to the CCO buffer that presents lower Fe^{3+}/Fe_{tot} (from 0.056 to 0.082; Table 5). The incorporation of Fe^{3+} at the $M(1)$ and $M(3)$ sites triggers the deprotonation of two OH^- hydroxyls from the two associated $O(3)$ sites in order to maintain the local charge balance (mechanism 2). Interestingly, in amphibole with lower TiO_2 content, as in the experiment 18-15HM (conducted at the same fO_2 conditions), this effect induced from local charge balance is not observed (Fig. 7b), suggesting that the dehydrogenation mechanism (2) is less pronounced, although the Fe^{3+}/Fe_{tot} ratio of 0.161 is the highest among our experiments (Table 5). This discrepancy can be explained by the different amount of the initial water content of the experiment or their experimental configuration (double- vs. triple-capsule techniques).

At comparable water content (Table 4), the experiment 17-9C shows higher TiO_2 content compared to run 17-4C (Fig. 7b), which can be ascribed to a greater incorporation of Ti^{4+} at $M(2,3)$ sites (which is not involved in the Ti oxo-substitution (1)) possibly via exchange vectors such as

$$^{M(2,3)}Ti^{4+} + {}^{T(1,2)}Al_2^{3+} {}^{M(2,3)}Mg_{-1}^{2+} + {}^{T(1,2)}Si_{-2}^{4+}$$

(Ti-Tschermak vector) and

$$^{M(2,3)}Ti^{4+} + {}^{T(1,2)}A1^{3+} {}^{M(2,3)}Al_{-1}^{3+} + {}^{T(1,2)}Si_{-1}^{4+}$$

(King et al., 1999; Tiepolo et al., 1999).

This interpretation is consistent with the highest ^{T}Al average content shown by amphiboles from experiment 17-9C (2.150 a.p.f.u.) among all experiments (Table 5). Moreover, the relative proportion of $^{M(2,3)}$Al in our amphiboles relative to the $^{M(2,3)}$Ti ranges from 1.2 to 1.6, falling within the range of relative proportions of the endmember exchanges proposed above.

6.3 Water contents in amphibole, H_2O and Cl partition coefficients between amphibole and liquid ($^{Amph/L}D_{H_2O}$, $^{Amph/L}D_{Cl}$)

The achievement of equilibrium conditions allows us to use the micro-Raman-derived water contents in amphibole and glasses to calculate the H_2O partition coefficients between amphibole and liquid ($^{Amph/L}D_{H_2O}$). This, in turn, provides an evaluation of the affinity of water in amphibole as a function of Cl content of the system. The calculated $^{Amph/L}D_{H_2O}$ (Table 4) ranges from 0.29 ± 0.06 in experiment 18-15HM to 0.52 ± 0.04 in experiment 17-9C (Fig. 8). No significant variation is observed as a function of variable fO_2 conditions. The calculated $^{Amph/L}D_{H_2O}$ indicates that water has a moderate affinity for amphibole. Data obtained from EMPA analyses were used to calculate the $^{Amph/L}D$ of Cl (Fig. 6a), which ranges from 0.248 ± 0.017 in experiment 17-7C to 0.439 ± 0.107 in experiment 17-4C (Table 4), with an average value of 0.38 ± 0.10 (Fig. 6a). Similar to $^{Amph/L}D_{H_2O}$, no significant variation is observed as a function of variable fO_2 conditions. The amphibole–liquid partition coefficient for Cl is highly debated in the literature, and a wide range of $^{Amph/L}D_{Cl}$ is provided (from 0.03 to 0.62; Dalou et al., 2014; Van den Bleeken and Koga, 2015; Bénard et al., 2017). Our data fall at the upper limit of the literature data (median at 0.26), supporting the moderate incompatibility of Cl for amphibole.

Compared to previous studies at water-undersaturated conditions that obtained $^{Amph/L}D_{H_2O}$ between 0.12 and 0.24 (Hauri et al., 2006), the present study suggests higher H_2O partition coefficients (Fig. 8a and b). It should be noted that the work of Hauri et al. (2006) is the only experimental work reporting $^{Amph/L}D_{H_2O}$. These experiments (runs 1442, 1446, and 1452) were performed at variable T ranging between 1000 and 1050 °C and P from 0.5 to 2.0 GPa, using a basanitic glass as starting material and producing amphibole with mainly Ti-pargasitic composition (Adam and Green, 1994). Unpublished experiment-derived SIMS (secondary ion mass spectrometry) analyses on $^{Amph/L}D_{H_2O}$ (Tiepolo,

Table 5. Calculated occupation of the amphibole T, B, and C sites and estimated Fe^{3+}/Fe_{tot}.

	17-4C	17-7C	17-9C	17-8HM	18-15HM
T site					
Si	5.891	6.004	5.810	5.851	5.946
Al	2.073	1.976	2.150	2.120	2.037
Ti	0.065	0.037	0.082	0.040	0.024
Sum	8.029	8.017	8.041	8.011	8.007
C site $M(1,2,3)$					
Al	0.923	0.762	0.916	0.778	0.722
Ti	0.620	0.469	0.720	0.652	0.508
Fe^{3+}	0.185	0.223	0.109	0.135	0.203
Mg	1.561	2.034	1.858	2.561	2.700
Fe^{2+}	1.813	1.552	1.527	0.917	0.885
Sum	5.103	5.040	5.130	5.042	5.019
B site $M(4)$					
Fe^{2+}	0.272	0.144	0.305	0.214	0.176
Mg	0.045	0.021	0.094	0.066	0.056
Ca	1.547	1.669	1.523	1.603	1.657
Na	0.120	0.161	0.053	0.106	0.102
Sum	1.983	1.996	1.976	1.988	1.990
Fe^{3+}/Fe_{tot}	0.082	0.116	0.056	0.106	0.161

Recalculated according to the formula $A_{0-1}B_2C_5T_8O_{22}W_2$ (23 oxygen atoms per formula unit, a.p.f.u.) using the method proposed in Li et al. (2020).

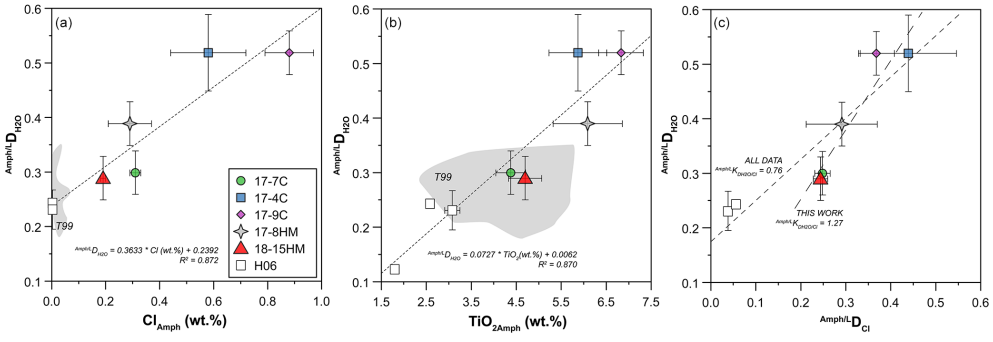

Figure 8. Correlation between $^{Amph/L}D_{H_2O}$ and Cl **(a)** and TiO_2 **(b)** contents (wt %) in amphibole. H06: data from Hauri et al. (2006); T99: data from Tiepolo (1999). The diagram in **(c)** shows the correlation between $^{Amph/L}D_{H_2O}$ and $^{Amph/L}D_{Cl}$, giving their exchange coefficient ($^{Amph/L}K_{DH_2O/Cl}$). $^{Amph/L}K_{DH_2O/Cl}$ obtained from this work is 1.27, although it becomes lower than unity considering all data (this study and data from Hauri et al., 2006).

1999) report an average value of 0.26 ± 0.04 ($n = 22$) for amphibole, characterized by significantly lower Cl (below 0.05 wt %) and variable TiO_2 contents (gray fields in Fig. 8a and b). These experiments were performed at equilibrium T from 950 to 1075 °C and fixed P of 1.4 GPa. The wide T range used for these experiments may explain the high variability in TiO_2 content of these amphiboles reported in Fig. 8b.

Remarkably, positive correlations are observed between $^{Amph/L}D_{H_2O}$ and Cl and TiO_2 contents in amphiboles (Fig. 8a and b) resembling the negative trends shown between the H_2O content in amphibole and its Cl and TiO_2 contents (Figs. 6b, 7b and c). Although our $^{Amph/L}D_{H_2O}$ has relatively higher uncertainty compared to SIMS data (Hauri et al., 2006), the correlation with Cl and TiO_2 can be linearly fitted, giving a good fit quality parameter, i.e., $R^2 =$

0.872 and 0.870 (Fig. 8), respectively. This evidence points to a significant effect of Cl (and TiO_2) in the hydrogenation of the amphibole, thus controlling its ability to incorporate water. Despite this evidence, a positive correlation between $^{Amph/L}D_{H_2O}$ and $^{Amph/L}D_{Cl}$ is shown in Fig. 8c, where the exchange coefficient between H_2O and Cl ($^{Amph/L}Kd_{H_2O/Cl} = {}^{Amph/L}D_{H_2O} / {}^{Amph/L}D_{Cl}$) for our data results in a preferential incorporation of water in amphibole compared to Cl ($^{Amph/L}Kd_{H_2O/Cl} \approx 1.27$). Remarkably, considering the data from Hauri et al. (2006), which extend the range of the $^{Amph/L}D_{H_2O}$ and $^{Amph/L}D_{Cl}$ towards lower values (Fig. 8c), the resulting $^{Amph/L}Kd_{H_2O/Cl}$ significantly changes ($^{Amph/L}Kd_{H_2O/Cl} \approx 0.76$), suggesting a preferential incorporation of Cl with respect to water. The explanation for such contrasting behavior is difficult to explain with the available data, and more detailed investigations are required to better unravel this conundrum.

6.4 The effect of Cl on the hydrogenation of amphibole

The measured water contents in both amphiboles and glasses in our experimental study are similar or lower compared to data provided by Hauri et al. (2006) (Fig. 7a); the calculated $^{Amph/L}D_{H_2O}$, however, is significantly higher (Fig. 8) and, interestingly, dependent on Cl (and TiO_2) contents in amphibole (Fig. 7b, c). In particular, our data highlight that for high Cl contents, dehydrogenation mechanisms are discouraged, and incorporation of water in amphibole is enhanced (Fig. 8). It should be noted that for comparable Cl content in amphibole, experiment 17-8HM performed at oxidized conditions ($\Delta FMQ = +1.7$) is characterized by higher $^{Amph/L}D_{H_2O}$ compared to experiment 17-7C, which runs at $\Delta FMQ = -2.6$ (Fig. 8a), suggesting a relevant role of the fO_2 condition of the system in influencing the affinity of water in amphibole.

The positive correlation between the Cl content in amphibole and $^{Amph/L}D_{H_2O}$ is unexpected as (i) Cl and water compete for the $O(3)$ occupancy, as clearly shown by the negative correlation between H_2O and Cl content in amphibole (Fig. 7c), and (ii) the presence of abundant Cl in the system lowers the fH_2, and, thus, the incorporation of H in amphibole should decrease or at least be limited (Popp et al., 1995b). The deviation of our data from these effects can therefore be explained by crystallographic reasons. Indeed, the presence of abundant Cl in amphibole greatly influences its crystal structure (Oberti et al., 1993; Hawthorne and Oberti, 2007; Oberti et al., 2007) and, in turn, might influence the Ti oxo-substitution (1) that regulates water incorporation in amphibole. Because $M(1)$ and $M(3)$ sites are coordinated by the $O(3)$ site, the occupancy of these three sites is interdependent. In particular, two $M(1)$ and one $M(3)$ sites are locally coordinated by two $O(3)$ sites, located above and below the strip of octahedra, respectively. The radius of Cl^- (1.81 Å; Shannon, 1976) is much larger compared to the other anions that can be hosted at the anionic sites ($F^- = 1.33$ Å, $OH^- = 1.37$Å, $O^{2-} = 1.40$ Å); therefore, the presence of Cl at the $O(3)$ site determines its expansion by stretching of the $<M(1)–O(3)>$ and $<M(3)–O(3)>$ bonds (Oberti et al., 1993; Hawthorne and Oberti, 2007). This expansion is facilitated by the presence of larger cations in $M(1)$ and $M(3)$, leading to the preferential incorporation of Mg^{2+} and, especially, Fe^{2+} at these sites, rather than smaller cations like Al^{3+}, Fe^{3+}, and Ti^{4+} that are instead relocated to the $M(2)$ sites (Giesting and Filiberto, 2016; Henry and Daigle, 2018). In particular, the presence of Cl^- at one of the two $O(3)$ sites does not allow the entrance of Ti^{4+} in $M(1)$, ultimately impeding the release of the OH^- hosted at the associated $O(3)$ site via reaction (1). Although the incorporation of Ti^{4+} at the $M(1)$ site is hampered at high Cl concentration, the observed increase in the TiO_2 content in amphibole associated with Cl (Fig. 6b) is explained by considering that a significant fraction of Ti^{4+} may also be hosted at the $M(2)$ site of the amphibole (Hawthorne et al., 1998; Tiepolo et al., 1999). Remarkably, this crystallographic feature appears to be linked to the fO_2 of the system and is more pronounced for experiments performed at high fO_2.

The coupled structural changes induced by the incorporation of Cl in amphibole also affect its trace element incorporation, as recently documented in a companying paper by Cannaò et al. (2022).

7 Concluding remarks

In this work we bring new knowledge of the effect of Cl on water incorporation in magmatic amphibole. Our results suggest that a significant discrimination in the uptake between H_2O and Cl is not apparent; their experimentally determined exchange coefficients are close to unity ($^{Amph/L}Kd_{H_2O/Cl}$ from 0.76 to 1.27). Notwithstanding, our findings reveal that at mantle depths the occurrence of Cl in the system increases the stability of a more hydrogenated amphibole, thus capable of incorporating higher amount of water. At geological timescales, this increases and widens the key role of amphibole as water storage and carrier in the lithosphere (Davidson et al., 2007; Smith, 2014).

Our study highlights the high potential of micro-Raman spectroscopy as a versatile analytical tool to quantify water in hydrous minerals crystallizing in various geological environments as well as in nominally anhydrous minerals (e.g., Thomas et al., 2008; Bolfan-Casanova et al., 2014; Weis et al., 2018; Martinek and Bolfan-Casanova, 2021). In particular, confocal micro-Raman spectroscopy allows non-destructive measurements, with minimal sample preparation, to be carried out rather quickly and at a modest cost. These advantages associated with its high spatial resolution down to the micrometer scale make this technique suitable for studying samples characterized by small grain size, polyphasic composition, and/or tiny volumes, including rare or valuable samples.

Data availability. All data derived from this research are presented in the enclosed tables and figures in the main text and the Supplement.

Supplement. The supplement related to this article is available online at: https://doi.org/10.5194/ejm-34-19-2022-supplement.

Author contributions. EC, MT, and PF conceptualized the project. EC and GC performed the experiments, and GC and FS carried out the micro-Raman analyses. Resources were provided by FS, MT, and PF. All authors discussed and interpreted the results. Acquisition of the financial support for the project was provided by PF. The manuscript was written by EC and FS with contributions by all co-authors.

Competing interests. The contact author has declared that neither they nor their co-authors have any competing interests.

Disclaimer. Publisher's note: Copernicus Publications remains neutral with regard to jurisdictional claims in published maps and institutional affiliations.

Special issue statement. This article is part of the special issue "Probing the Earth: experiments and mineral physics at mantle depths". It is not associated with a conference.

Acknowledgements. This work was supported by the Italian Ministry of Education, University and Research (MIUR), "Programma di Rilevante Interesse Nazionale" project "Melt-rock reaction and melt migration in the MORB mantle through combined natural and experimental studies" (grant no. PRIN2015C5LN35). Federica Schiavi thanks Nathalie Bolfan-Casanova for constructive discussion, Didier Laporte for providing an amphibole standard, and Claire Fonquernie for CHNS analyses at the LMV. Giulia Casiraghi thanks the University of Milan for providing financial support through the "Thesis-abroad" grant, which helped cover the expenses for the period spent at the LMV. Further, the authors thank Fernando A. Camara (University of Milan) for his useful insights on amphibole crystallography. Constructive reviews by Roland Stalder and Chao Zhang as well as manuscript handling by Max Wilke (associated editor) and Elisabetta Rampone (chief editor) have been much appreciated.

Financial support. This research has been supported by the Ministero dell'Istruzione, dell'Università e della Ricerca (grant no. PRIN2015C5LN35).

Review statement. This paper was edited by Max Wilke and reviewed by Chao Zhang and Roland Stalder.

References

Adam, J. and Green, T. H.: The effects of pressure and temperature on the partitioning of Ti, Sr and REE between amphibole, clinopyroxene and basanitic melts, Chem. Geol., 117, 219–233, 1994.

Adam, J., Oberti, R., Cámara, F., and Green, T. H.: An electron microprobe, LAM-ICP-MS and single-crystal X-ray structure refinement study of the effects of pressure, melt-H_2O concentration and fO_2 on experimentally produced basaltic amphiboles, Eur. J. Mineral., 19, 641–655, https://doi.org/10.1127/0935-1221/2007/0019-1750, 2007.

Benard, A., Koga, K. T., Shimizu, N., Kendrick, M. A., Ionov, D. A., Nebel, O., and Arculus, R. J.: Chlorine and fluorine partition coefficients and abundances in sub-arc mantle xenoliths (Kamchatka, Russia): Implications for melt generation and volatile recycling processes in subduction zones, Geochim. Cosmochim. Ac., 199, 324–350, 2017.

Bolfan-Casanova, N., Montagnac, G., and Reynard, B.: Measurement of water contents in olivine using Raman spectroscopy, Am. Mineral., 99, 149–156, 2014.

Campbell, I. and Schenk, E. T.: Camptonite Dikes Near Boulder Dam, Arizona, Am. Mineral., 35, 671–692, 1950.

Cannaò E., Tiepolo, M., Borghini, G., Langone, A., and Fumagalli, P.: The influence of oxygen fugacity and chlorine on amphibole/liquid trace element partitioning at upper mantle conditions, Eur. J. Mineral., accepted, 2022.

Cawthorn, R. G.: The amphibole peridotite-metagabbro complex, Finero, northern Italy, J. Geol., 83, 437–454, 1975.

Clowe, C. A., Popp, R. K, and Fritz, S. J.: Experimental investigation of the effect of oxygen fugacity on ferric-ferrous ratios and unit-cell parameters of four natural clinoamphiboles, Am. Mineral., 73, 487–499, 1988.

Coltorti, M., Bonadiman, C., Faccini, B., Grégoire, M., O'Reilly, S. Y., and Powell, W.: Amphiboles from suprasubduction and intraplate lithospheric mantle, Lithos, 99, 68–84, 2007.

Dalou, C., Koga, K. T., Le Voyer, M., and Shimizu, N.: Contrasting partition behavior of F and Cl during hydrous mantle melting: implications for Cl/F signature in arc magmas, Progress in Earth and Planetary Science, 1, 26, https://doi.org/10.1186/s40645-014-0026-1, 2014.

Dautria, J. M., Liotard, J. M., Cabanes, N., Girod, M., and Briqueu L.: Amphibole-rich xenoliths and host alkali basalts: petrogenetic constraints and implications on the recent evolution of the upper mantle beneath Ahaggar (Central Sahara, Southern Algeria), Contrib. Mineral. Petrol., 95, 133–144, 1987.

Davidson, J., Turner, S., Handley, H., Macpherson, C., and Dosseto, A.: Amphibole "sponge" in arc crust?, Geology, 35, 787–790, https://doi.org/10.1130/G23637A.1, 2007.

Dawson, J. B. and Smith, J. V.: Upper mantle amphiboles: a review, Mineral. Mag., 45, 35–46, 1982.

Deer, W. A., Howie, R. A., and Zussman, J. (Eds.): Double chain silicates (Rock-forming minerals), v. 2B, 2nd edition, Geological Society of London, 1997.

Demény, A., Vennemann, T. W., Homonnay, Z., Milton, A., Embey-Isztin, A., and Nagy, G.: Origin of amphibole megacrysts in the Pliocene-Pleistocene basalts of the Carpathian-Pannonian region, Geolog. Carpath., 56, 179–189, 2005.

Demény, A., Vennemann, T. W., Harangi, S., Homonnay, Z., and Fórizs, I.: H_2O-δD-FeIII relations of dehydrogenation and de-

hydration processes in magmatic amphiboles, Rapid Commun. Mass Spectrom., 20, 919–925, 2006.

Dyar, M. D., McGuire, A. V., and Mackwell, S. J.: Fe^{3+}/H^{+} and D/H in kaersutites – Misleading indicators of mantle source fugacities, Geology, 20, 565–568, 1992.

Ernst, W. G.: Petrochemical study of lherzolitic rocks from the Western Alps, J. Petrol., 19, 341–392, 1978.

Fabriès, J., Figuero, O., and Lorand, J. P.: Petrology and Thermal History of Highly Deformed Mantle Xenoliths from the Montferrier Basanites, Languedoc, Southern France: A Comparison with Ultramafic Complexes from the North Pyrenean Zone, J. Petrol., 28, 887–919, 1987.

Field, S. W., Haggerty, S. E., and Erlank, A. J.: Subcontinental metasomatism in the region of Jagersfontein, South Africa, in: Kimberlites and related rocks, Geological Society of Australia, Special Publications, 14, 771–783, 1989.

Francis, D. M.: The origin of amphibole in lherzolite xenoliths from Nunivak Island, Alaska, J. Petrol., 17, 357–378, 1976.

Frezzotti, M. L., Ferrando, S., Peccerillo, A., Petrelli, M., Tecce, F., and Perucchi, A.: Chlorine-rich metasomatic H_2O–CO_2 fluids in amphibole-bearing peridotites from Injibara (Lake Tana region, Ethiopian plateau): nature and evolution of volatiles in the mantle of a region of continental flood basalts, Geochim. Cosmochim. Ac., 74, 3023–3039, 2010.

Ganguly, J. and Newton, R. C.: Thermal stability of chloritoid at high pressure and relatively high oxygen fugacity, J. Petrol., 9, 444–466, 1968.

Giesting, P. A, and Filiberto, J.: The formation environment of potassic-chloro-hastingsite in the nakhlites MIL 03346 and pairs and NWA 5790: Insights from terrestrial chloro-amphibole, Meteorit. Planet. Sci., 51, 2127–2153, 2016.

Green D. H.: The petrogenesis of the high temperature peridotite intrusion in the Lizard Area, Cornwall, J. Petrol., 5, 134–188, 1964.

Griffin, W. L., Wass, S. Y., and Hollis, J. D.: Ultramafic Xenoliths from Bullenmerri and Gnotuk Maars, Victoria, Australia: Petrology of a Sub-Continental Crust-Mantle Transition, J. Petrol., 25, 53–87, 1984.

Hauri, E. H., Gaetani, G. A., and Green, T. H.: Partitioning of water during melting of the Earth's upper mantle at H_2O-undersaturated conditions, Earth Planet. Sc. Lett., 248, 715–734, 2006.

Hawthorne, F. C. and Oberti, R.: Amphiboles: Crystal Chemistry, Rev. Mineral. Geochem., 67, 1–54, https://doi.org/10.1515/9781501508523-002, 2007.

Hawthorne, F. C., Oberti, R., Zanetti, A., and Czamanske, G. K.: The role of Ti in hydrogen-deficient amphiboles: sodic-calcic and sodic amphiboles from Coyote Peak, California, Can. Mineral., 36, 1253–1265, 1998.

Hawthorne, F. C., Oberti, R., Harlow, G. E., Maresch, W. V., Martin, R. F., Schumacher, J. C., and Welch, M. D.: Nomenclature of the amphibole supergroup, Am. Mineral., 97, 2031–2048, 2012.

Henry, D. J. and Daigle, N. M.: Chlorine incorporation into amphibole and biotite in high-grade iron-formations: Interplay between crystallography and metamorphic fluids, Am. Mineral., 103, 55–68, 2018.

Ionov, D. A. and Hofmann, A. W.: Nb-Ta-rich mantle amphiboles and micas: Implications for subduction-related metasomatic trace element fractionations, Earth Planet. Sc. Lett., 131, 341–356, 1995.

Johannes, W. and Bode, B:. Loss of iron to the Pt-container in melting experiments with basalts and a method to reduce it, Contrib. Mineral. Petrol., 67, 221–225, https://doi.org/10.1007/BF01046578, 1978.

King, P. L., Hervig, R. L., Holloway, J. R., Venneman, T. W., and Righter, K.: Oxy-substitution and dehydrogenation in mantle-derived amphibole megacrysts, Geochim. Cosmochim. Ac., 63, 3635–3651, 1999.

Leake, B. E., Woolley, A. R., Arps, C. E. S., Birch, W. D., Gilbert, M. C., Grice, J. D., Hawthorne, F. C., Kato, A., Kisch, H. J., Krivovichev, V. G., Linthout, K., Laird, J., Mandarino, J. A., Maresch, W. V., Nickel, E. H., Rock, N. M. S., Schumacher, J. C., Smith, D. C., Stephenson, N. C. N., Ungaretti, L., Whittaker, E. J. W., and Youzhi, G.: Nomenclature Of Amphiboles: Report Of The Subcommittee On Amphiboles Of The International Mineralogical Association, Commission On New Minerals And Mineral Names, Can. Mineral., 35, 219–246, 1997.

Leissner, L., Schlüter, J., Horn, I., and Mihailova, B.: Exploring the potential of Raman spectroscopy for crystallochemical analyses of complex hydrous silicates: I. Amphiboles, Am. Mineral., 100, 2682–2694, 2015.

Li, X., Zhang, C., Behrens, H., and Holtz, F.: Calculating amphibole formula from electron microprobe analysis data using a machine learning method based on principal components regression, Lithos, 362–363, 105469, https://doi.org/10.1016/j.lithos.2020.105469, 2020.

Libowitzky, E. and Rossman, G. R.: Principles of quantitative absorbance measurements in anisotropic crystals, Phys. Chem. Miner., 23, 319–327, 1996.

Makino, K., Tomita, K., and Suwa, K. Effect of chlorine on the crystal structure of a chlorine-rich hastingsite, Mineral. Mag., 57, 677–685, 1993.

Mandler, B. E. and Grove T. L.: Controls on the stability and composition of amphibole in the Earth's mantle, Contrib. Mineral. Petrol., 171, 1–20, https://doi.org/10.1007/s00410-016-1281-5, 2016.

Marocchi, M., Hermann, J., and Morten, L.: Evidence for multistage metasomatism of chlorite-amphibole peridotites (Ulten Zone, Italy): Constraints from trace element compositions of hydrous phases, Lithos, 99, 85–104, 2007.

Martinek, L. and Bolfan-Casanova, N.: Water quantification in olivine and wadsleyite by Raman spectroscopy and study of errors and uncertainties, Am. Mineral., 106, 570–580, 2021.

Matjuschkin, V., Brooker, R. A., Tattitch, B., Blundy, J. D., and Stamper, C. C.: Control and monitoring of oxygen fugacity in piston cylinder experiments, Contrib. Mineral. Petrol., 169, 9, https://doi.org/10.1007/s00410-015-1105-z, 2015.

Mayer, B., Jung, S., Romer, R. L., Pfänder, J. A., Klügel, A., Pack, A., and Gröner, E.: Amphibole in alkaline basalts from intraplate settings: implications for the petrogenesis of alkaline lavas from the metasomatised lithospheric mantle, Contrib. Mineral. Petrol., 167, 989, https://doi.org/10.1007/s00410-014-0989-3, 2014.

Médard, E. and Grove T. L.: The effect of H_2O on the olivine liquidus of basaltic melts: experiments and thermodynamic models, Contrib. Mineral. Petrol., 155, 417–432, 2008.

Medaris, L. G.: Petrogenesis of the Lien Peridotite and associated eclogites, Almklovdalen, Western Norway, Lithos, 13, 339–153, 1980.

Medaris, L. G.: A geothermobarometric investigation of garnet peridotites in the western gneiss region of Norway, Contrib. Mineral. Petrol., 87, 72–86, 1984.

O'Reilly, S. Y. and Griffin, W. L.: Mantle metasomatism beneath western Victoria, Australia: I. Metasomatic processes in Cr-diopside lherzolites, Geochim. Cosmochim. Ac., 52, 433–447, 1988.

Obata, M.: The Ronda peridotite: garnet-, spinel-, and plagioclase-lherzolite facies and the $P-T$ trajectories of a high temperature mantle intrusion, J. Petrol., 21, 533–572, 1980.

Obata, M. and Morten, L.: Transformation of spinel lherzolite to garnet lherzolite in ultramafic lenses of the Austridic Crystalline Complex, northern Italy, J. Petrol., 28, 599–623, 1987.

Oberti, R., Ungaretti, L., Cannillo, E., and Hawthorne, F. C.: The mechanism of Cl incorporation in amphibole, Am. Mineral., 78, 746–752, 1993.

Oberti, R., Hawthorne, F. C., Cannillo, E., and Cámara, F.: Long-Range Order in Amphiboles, Rev. Mineral. Geochem., 67, 125–171, 2007.

Peters, S. T., Troll, V. R., Weis, F. A., Dallai, L., Chadwick, J. P., and Schulz, B.: Amphibole megacrysts as a probe into the deep plumbing system of Merapi volcano, Central Java, Indonesia, Contrib. Mineral. Petrol., 172, 16, https://doi.org/10.1007/s00410-017-1338-0, 2017.

Piper, D. J., Pe-Piper, G., Anastasakis, G., and Reith, W.: The volcanic history of Pyrgousa – volcanism before the eruption of the Kos Plateau Tuff, B. Volcanol., 81, 32, https://doi.org/10.1007/s00445-019-1290-0, 2019.

Popp, R. K., Virgo, D., Yoder Jr., H. S., Hoering, T. C., and Phillips, M. W.: An experimental study of phase equilibria and Fe oxy-component in kaersutitic amphibole: Implications for the fH_2 and aH_2O in the upper mantle, Am. Mineral., 80, 534–548, 1995a.

Popp, R. K., Virgo, D., and Phillips, M. W.: H deficiency in kaersutitic amphiboles: Experimental verification, Am. Mineral., 80, 1347–1350, 1995b.

Popp, R. K., Hibbert, H. A., and Lamb, W. M.: Oxy-amphibole equilibria in Ti-bearing calcic amphiboles: Experimental investigation and petrologic implications for mantle-derived amphiboles, Am. Mineral., 91, 54–66, 2006.

Press, S., Witt, G., Seck, H. A., Ionov, D., and Kovalenko, V. I.: Spinel peridotite xenoliths from the Tariat Depression, Mongolia. I. Major element chemistry and mineralogy of a primitive mantle xenolith suite, Geochim. Cosmochim. Ac., 50, 2587–2599, 1986.

Rampone, E. and Morten, L.: Records of crustal metasomatism in the garnet peridotites of the Ulten Zone (Upper Austroalpine, Eastern Alps), J. Petrol., 42.1, 207–219, 2001.

Schiavi, F., Bolfan-Casanova, N., Withers, A. C., Médard, E., Laumonier, M., Laporte, D., and Gómez-Ulla, A.: Water quantification in silicate glasses by Raman spectroscopy: Correcting for the effects of confocality, density and ferric iron, Chem. Geol., 483, 312–331, 2018.

Schmidt, M. W. and Ulmer, P: A rocking multianvil: elimination of chemical segregation in fluid-saturated high-pressure experiments, Geochim. Cosmochim. Ac., 68, 1889–1899, 2004.

Seyler, M. and Mattson, P. H.: Petrology and thermal evolution of the Tinaquillo peridotite (Venezuela), J. Geophys. Res., 94, 7629–7660, 1989.

Shannon, R. D.: Revised effective ionic radii and systematic studies of interatomic distances in halides and chalcogenides, Acta Crystallogr. Sect. A Cryst. Phys. Diffr. Theor. Gen. Crystallogr., 32, 751–767, 1976.

Smith, D. J.: Clinopyroxene precursors to amphibole sponge in arc crust, Nat. Comm., 5, 4329, https://doi.org/10.1038/ncomms5329, 2014.

Takahashi, E.: Thermal history of lherzolite xenoliths. I. Petrology of lherzolite xenoliths from the Ichinomegata crater, Oga Peninsula, northeast Japan, Geochim. Cosmochim. Ac., 44, 1643–1658, 1980.

Thomas, S. M., Thomas, R., Davidson, P., Reichart, P., Koch-Müller, M., and Dollinger, G.: Application of Raman spectroscopy to quantify trace water concentrations in glasses and garnets, Am. Mineral., 93, 1550–1557, 2008.

Tiepolo, M.: Determinazione sperimentale dei coefficienti di distribuzione solido/liquido in anfiboli di mantello: ruolo del controllo cristallochimico, PhD Thesis, Università di Pavia, 314 pp., 1999 (in Italian).

Tiepolo, M., Zanetti, A., and Oberti, R.: Detection, crystal-chemical mechanism and petrological implications of $^{[6]}Ti^{4+}$ partitioning in pargasite and kaersutite, Eur. J. Mineral., 11, 345–354, https://doi.org/10.1127/ejm/11/2/0345, 1999.

Tiepolo, M., Vannucci, R., Bottazzi, P., Oberti, R., Zanetti, A., and Foley, S.: Partitioning of rare earth elements, Y, Th, U, and Pb between pargasite, kaersutite, and basanite to trachyte melts: Implications for percolated and veined mantle, Geochem. Geophy. Geosy., 1, 1039, https://doi.org/10.1029/2000GC000064, 2000.

Ulmer, P. and Luth, R. W.: The graphite-COH fluid equilibrium in P, T, fO_2 space: An experimental determination to 30 kbar and 1600 °C, Contrib. Mineral. Petrol., 106, 265–272, 1991.

Van den Bleeken, G. and Koga, K. T.: Experimentally determined distribution of fluorine and chlorine upon hydrous slab melting, and implications for F–Cl cycling through subduction zones, Geochim. Cosmochim. Ac., 171, 353–373, 2015.

Vannucci, R., Piccardo, G. B., Rivalenti, G., Zanetti, A., Rampone, E., Ottolini, L., Oberti, R., Mazzucchelli, M., and Bottazzi, P.: Origin of LREE-depleted amphiboles in the subcontinental mantle, Geochim. Cosmochim. Ac., 59, 1763–1771, 1995.

Varne, R.: Hornblende lherzolite and the upper mantle, Contrib. Mineral. Petrol., 27, 45–51, 1970.

Wedepohl, K. H.: Die chemische Zussamensetzung der basaltischen Gesteine der nordlichen Hessichen Senke und ihrer Umgebung, Geol. Jahrb. Hessen, 111, 261–302, 1983.

Weis, F. A., Lazor, P., and Skogby, H.: Hydrogen analysis in nominally anhydrous minerals by transmission Raman spectroscopy, Phys. Chem. Miner., 45, 597–607, 2018.